Effect of ion ∇B drift direction on density fluctuation poloidal flow and flow shear

C. Fenzi,[a] G. R. McKee, and R. J. Fonck
University of Wisconsin-Madison, Madison, Wisconsin 53706

K. H. Burrell, T. N. Carlstrom, and R. J. Groebner
General Atomics, P.O. Box 85608, San Diego, California 92186-5608

(Received 23 November 2004; accepted 25 March 2005; published online 26 May 2005)

The divertor magnetic geometry has a significant effect on the poloidal velocity and resulting velocity shear of turbulent density fluctuations in the outer region of *L*-mode tokamak plasmas, as determined via two-dimensional measurements of density fluctuations with beam emission spectroscopy on DIII-D [J. L. Luxon, Nucl. Fusion **42**, 614 (2002)]. Plasmas with similar parameters, except that in one case the ion ∇B drift points towards the divertor *X* point (lower-single-null, LSN), and in the other case, the ion ∇B drift points away from the divertor *X* point (upper-single-null, USN), are compared. Inside $r/a=0.9$, the turbulence characteristics (density fluctuation amplitude, flow direction, correlation lengths) are similar in both cases, while near $r/a=0.92$, a dramatic reversal of the poloidal velocity of turbulent eddies relative to the core flow direction is observed in plasmas with the ion ∇B drift pointing towards the divertor *X* point. No such velocity reversal is observed in plasmas with the ion ∇B drift pointing away from the divertor *X* point. This poloidal velocity reversal results in a significantly larger local shear in the poloidal velocity of density fluctuations in plasmas with the ion ∇B drift pointing towards the divertor *X* point. Additionally, these plasmas locally exhibit significant dispersion with two distinct and counterpropagating turbulence modes. Likewise, the radial correlation length of the density fluctuations is reduced in these plasmas, consistent with biorthogonal decomposition measurements of dominant turbulence structures. The naturally occurring density fluctuation poloidal velocity shear in these LSN plasmas may facilitate the *L-H* transition that occurs at an input power of roughly one-half to one-third that of corresponding plasmas with the ion ∇B drift pointing away from the *X* point. © *2005 American Institute of Physics*. [DOI: 10.1063/1.1915349]

I. INTRODUCTION

A detailed understanding of the *L*-mode to *H*-mode transition physics, as well as the associated transport improvement, is crucial to optimizing tokamak performance. By injecting sufficient power, plasmas undergo a spontaneous transition from a low confinement mode (*L*-mode) to a higher confinement mode (*H*-mode).[1] It has been demonstrated that the mechanism for *L*- to *H*-mode transition is a rapid suppression of turbulence resulting from increased $E\times B$ shear.[2–5] The injected power at which the *L-H* transition occurs is not well understood, though it is well known empirically for a given experimental configuration and set of plasma parameters. Of particular interest is predicting the necessary transition power in future large experimental devices to ensure that they can be operated in higher performance *H*-mode conditions. Recent studies have focused on dimensionless scaling analyses, which have provided useful guidance.[6]

Generally, the *H*-mode transition is facilitated by additional heating, hence a higher temperature and less collisional edge plasma. Nevertheless, it has been a difficult task to identify critical edge parameters at the *L-H* transition which are not related to the input power,[7–10] though a recent theoretical study has identified a parameter proportional to $T_e/\sqrt{L_n}$ as a criteria for transition from *L* mode to *H* mode that shows good agreement with experimental measurements.[11] A wide range of theories of the *L-H* transition is reviewed in Ref. 12. Experimentally, it has been observed that the ion ∇B drift direction relative to the dominant *X* point has a dramatic effect on the *L-H* transition power threshold.[13–15] In DIII-D, the power threshold is lower by a factor of 2–3 when the ion ∇B drift is directed towards the *X* point[13] relative to that when the ion ∇B drift is pointed away from the *X* point.

Motivated by the recognition of the role of turbulence suppression in causing the *L-H* transition, and observing the strong dependence of the transition power on the magnetic geometry, recent experiments on DIII-D have explored turbulence characteristics near the critical edge region as a function of the magnetic geometry. In these experiments, the input power was kept constant at just below the *L-H* power threshold for plasmas with the ion ∇B drift towards the *X* point for both magnetic configurations. Two-dimensional measurements of density fluctuations were obtained using the beam emission spectroscopy (BES) diagnostic. The aim of this paper is to compare and contrast the edge fluctuation dynamics between configurations where the ion ∇B drift is away from and towards the *X* point (this is accomplished by

[a]Present address: Association Euratom-CEA sur la Fusion Contrôlée, CEA Cadarache, France.

upper- and lower-single-null-divertor configurations, respectively). In particular, the velocity and velocity shear of the turbulent density fluctuations are examined and contrasted. By velocity of the turbulent density fluctuations, we refer to the time-averaged poloidal velocity of turbulent eddies as observed in the laboratory frame, as opposed to fluid (bulk plasma) flow or the $E\times B$ flow. Turbulent eddies are generally expected to propagate poloidally in the laboratory at or near the $E_r\times B_T$ velocity, though the intrinsic mode velocity (of order of the diamagnetic velocities) can become significant, especially near the plasma edge. These effects can lead to significant differences between the $E\times B$ and density fluctuation poloidal velocities. Furthermore, this density fluctuation flow also exhibits significant dispersion (wave number and/or frequency dependence) in some configurations, and so the frequency or wave number range is specified as necessary. Details about the *L-H* transition physics as well as the ∇B drift experiment itself are addressed in Ref. 15.

This paper is organized as follows: Section II provides experimental evidence for the existence of a large fluctuation velocity shear at the plasma edge when the ion ∇B drift is directed towards the *X*-point location, in contrast with the configuration where the ion ∇B drift is away from it. Section III presents the fluctuation characteristics for both configurations and illustrates the statistical properties of the fluctuations across the observed shear zone. Furthermore, a biorthogonal decomposition analysis is applied to the data in order to further investigate the spatial and temporal dynamics of the edge fluctuations. The question of the role of the density fluctuation velocity shear versus the $E_r\times B_T$ shear is discussed in Sec. IV, as well as its possible effect on the *L-H* transition. Finally, a summary is presented in Sec. V.

II. ION ∇B DRIFT DIRECTION EFFECT ON FLUCTUATIONS

The density fluctuation measurements discussed here were obtained with the BES diagnostic installed on DIII-D.[16] The system measures the Doppler-shifted D_α light emitted from an injected high power D° neutral beam, and provides measurements of spatially localized long-wavelength density fluctuations in the wave number range $k<3$ cm^{-1} (typically associated with anomalous energy and particle transport in the edge and core plasma regions), with a 1 cm radial and poloidal resolution.[17] The data are sampled at 1 MHz and frequency filtered over the region of broadband fluctuations in order to isolate the broadband turbulent modes, and reject photon and electronic noise at other frequencies. We examine *L*-mode plasmas in the upper- (lower-) single-null-divertor configuration, in which the ion ∇B drift direction is away from (towards) the magnetic field *X*-point location. The 32 spatial channels have been arranged in a two-dimensional (2D) 5×6 channel grid so as to image a 5×6 cm^2 (radial $\times$poloidal) region in the plasma poloidal cross section, in the radial range $0.87\leqslant\rho\leqslant 1.0$, near the outer midplane. This BES configuration thus provides visualization of 2D large-scale, transient, and coherent (localized in time and in space) structures in density turbulence.[18,19] The deployment of spatial channels with respect to the plasma cross section is shown in Fig. 1.

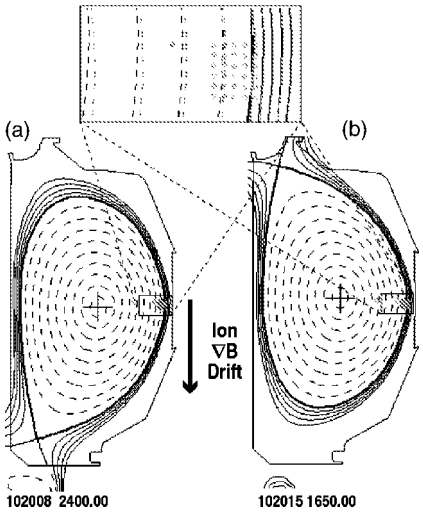

FIG. 1. Magnetic equilibrium for the (a) lower-single-null (LSN, ion ∇B drift towards *X* point) and (b) upper-single-null (USN, ion ∇B drift away from *X* point); inset shows BES channel locations for fluctuation imaging and velocity analysis.

The neutral beam input power for these experiments is 1.9 MW [just below the *L-H* power threshold for lower-single-null (LSN) plasmas] with operational parameters $I_p=1.0$ MA, $B_T=-2.1$ T, $\langle n_e\rangle=2.5\times 10^{19}$ m^{-3}. All neutral beams are injected in the co-current direction, which is antiparallel to the toroidal magnetic field. The same injected neutral beam power was used for both magnetic configurations. A slight increase in power would cause the LSN plasmas to undergo a *L-H* transition, while the upper-single-null (USN) plasmas would require significantly greater injected power before a *L-H* transition would occur. Profiles of measured edge parameters are shown in Fig. 2 for the electron density, ion and electron temperatures, electron pressure, carbon impurity density, and radial electric field. These profiles are generally similar between the upper-single-null and lower-single-null configurations,[15] suggesting that differences in these edge plasma parameters may not explain the large difference in *L-H* transition power threshold. The electron pressure shows a slight difference, being modestly lower in the USN configuration, though this difference is not convincingly outside of the uncertainty of the measurements; the carbon impurity density shows a significant difference, not thought to be directly relevant to the transition physics. A possible correlation between these small differences and the theoretical model discussed in Ref. 11 is discussed in Sec. IV.

The local density fluctuation spectral characteristics are compared in Fig. 3. The coherency and cross-phase spectra of the density fluctuations, calculated between two poloidally separated channels ($\Delta Z=2$ cm), are compared between the two magnetic configurations. These spectra (and all turbulence measurements presented in this paper) are ensemble averaged over a few hundred milliseconds to provide good statistics, and thus reflect the time-averaged, or mean characteristics of the density turbulence. In the LSN configura-

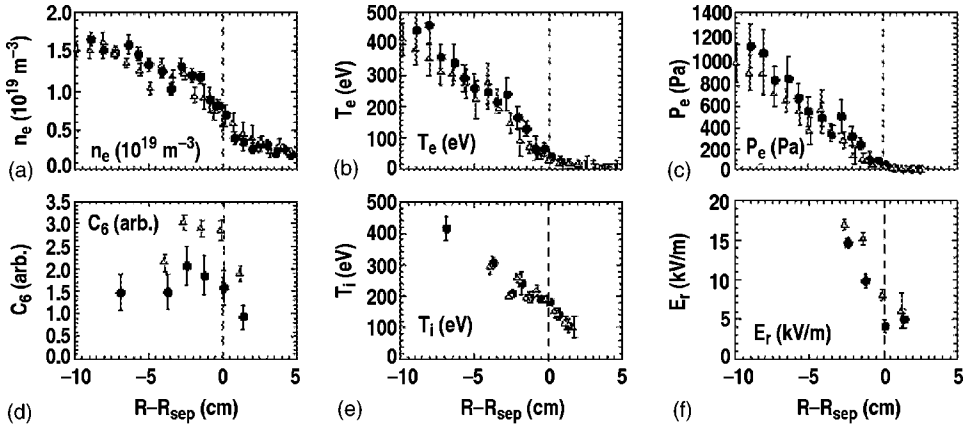

FIG. 2. Edge plasma profiles for USN (open symbols) and LSN (closed symbols) plasmas: (a) electron density, (b) electron temperature, (c) electron pressure, (d) carbon density, (e) ion temperature, (f) radial electric field (reproduced with permission from Ref. 15).

tion and at the innermost array location ($\rho \approx 0.87$), coherency spectra exhibit a double hump shape with oppositely directed phase shifts, corresponding to two counterpropagating modes for the turbulence [Figs. 3(a) and 3(d)]. A positive and increasing cross phase is associated with the higher frequency band ($f=40$–200 kHz), indicating that these fluctuations propagate in the ion diamagnetic direction, as seen in the laboratory frame. Fluctuations associated with the lower frequency mode ($f=10$–30 kHz) propagate in the electron diamagnetic direction (negative cross-phase). In the USN configuration, this dual counterpropagating mode feature is not observed, and there is no change in the direction of propagation of the fluctuations across the turbulent spectrum. The turbulence is single mode and drifts in the ion diamagnetic direction. At $\rho \approx 0.90$, the LSN case [Figs. 3(b) and 3(e)] more clearly shows the dual counterpropagating modes, with the break point near 50 kHz, though the coherency spectra suggest the modes in fact overlap in frequency. The USN case again shows the single mode structure. At $\rho \approx 0.93$ [Figs. 3(c) and 3(f)], the spectra show a striking distinction, with oppositely directed phase across the frequency range of the measured broadband fluctuations, corresponding to a flow reversal; the LSN configuration exhibits fluctuations propagating in the electron diamagnetic direction (negative cross phase), though there still appear to be two spectrally overlapping modes here propagating in the same direction at slightly different velocities. There is again no change in direction (sign of phase) for the USN configuration at that location relative to nearby radial locations. Finally, beyond that flow reversal zone (not shown), the LSN fluctuations drift again in the ion diamagnetic direction, and the USN fluctuations reverse direction near the separatrix.

Two-dimensional velocity-field plots of the density fluctuations are shown in Fig. 4 for both USN and LSN configurations. The k-averaged poloidal group velocities have been inferred from time-delay correlation analyses[20] between channels separated poloidally by about 1 cm. The velocity is measured as $v_\theta = \Delta Z / \tau_{\max}$, where $\tau_{\max}$ is the time delay at which maximum correlation occurs. Note that in the LSN configuration, where the two counterpropagating modes are observed, the group velocities have been evaluated by filtering the higher frequency mode that dominates the power spectrum ($f=50$–180 kHz), though in this case where two counterpropagating modes are present, the eddy flow velocity clearly depends on which mode or frequency band is being analyzed.

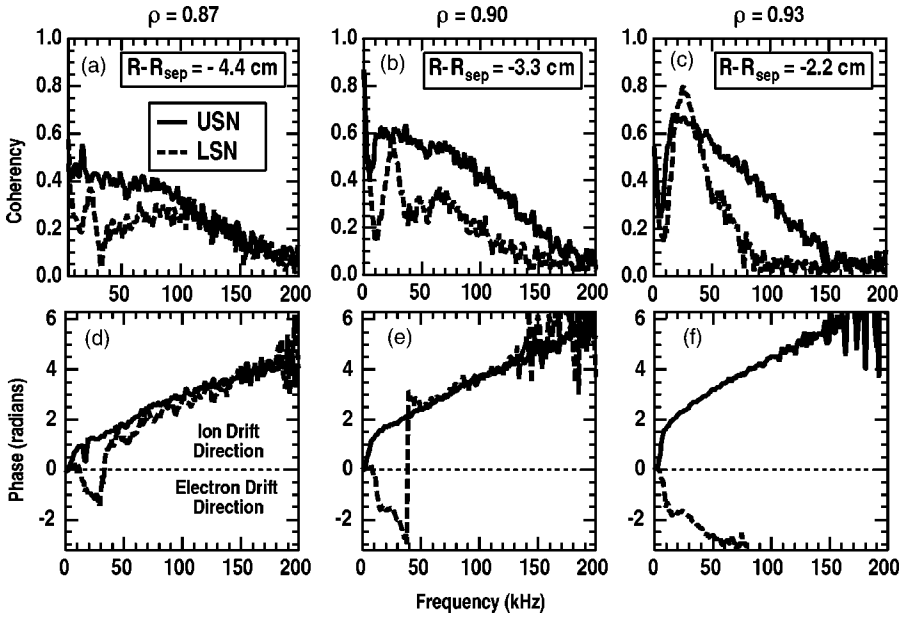

FIG. 3. Comparison of the turbulence coherency and cross-phase spectra for two poloidally separated channels ($\Delta Z=2$ cm) in the LSN and USN plasmas at three radial locations. The USN plasma exhibits a uniformly positive and increasing cross phase with frequency, indicating eddy flow in the ion diamagnetic direction (in laboratory frame), while the LSN plasma exhibits counterpropagating modes and gradual reversal of flow by $r/a=0.93$; note that some phase data are offset modulo 2π to avoid the visual discontinuity of 2π phase jumps.

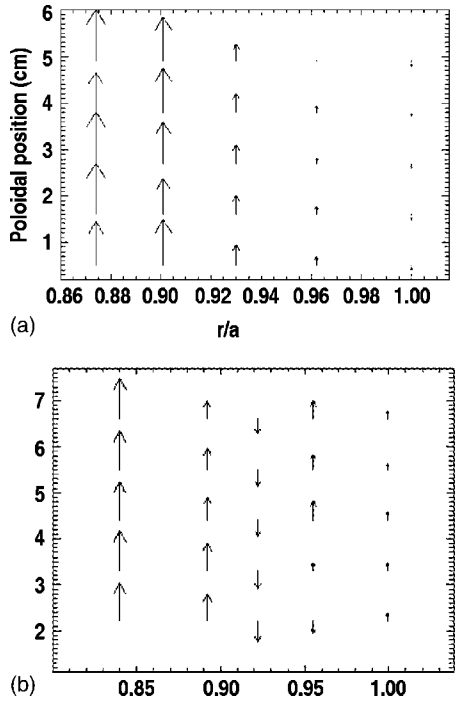

FIG. 4. Two-dimensional time-averaged density fluctuation velocity field for both configurations at the measurement location just below the outer midplane: (a) upper-single-null and (b) lower-single-null. Note the flow reversal near $\rho=0.92$ in the lower-single-null configuration. Largest arrows indicate velocities of near 5 km/s. In cases of dual modes (LSN), the dominant mode is chosen for velocity measurements ($f=50$–200 kHz). Here, vertically upward is the ion diamagnetic direction, and vertically downward is the electron diamagnetic direction.

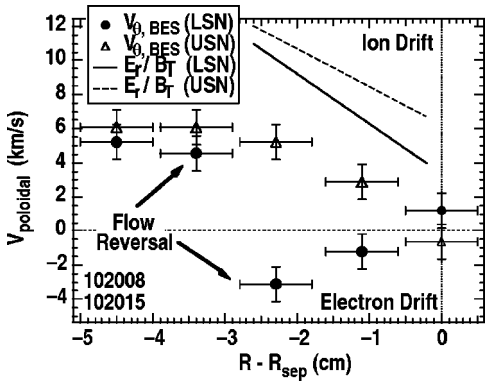

FIG. 5. Comparison of the turbulence poloidal group velocities (inferred from time delay correlation analyses) in USN and LSN plasmas, showing sharp reversal near $R-R_{\mathrm{sep}}=-3$ cm in the LSN plasma. $E_r\times B_T$ velocities obtained from CER measurements are shown for comparison.

The poloidal group velocity decreases from the plasma core towards the edge. It should be noted that in these experiments, the neutral beams are injected in the same direction as the plasma current. The injected angular momentum from the beams causes an electric field such that the resulting $E\times B$ drift is in the ion diamagnetic direction. The $E\times B$ velocity in DIII-D is typically much larger than the intrinsic mode velocity (of the order of diamagnetic velocities), except near the edge regions, which are being examined here, where they can be comparable. In the USN configuration, the flow direction gradually reduces from the core to the edge and reverses direction near the separatrix. In the LSN configuration, a striking fluctuation flow reversal, or change of sign (relative to the velocity deeper in the core) is observed in the range $\rho=0.9$–0.93, 2–3 cm inside the separatrix, as previously indicated by the cross-phase spectral analysis (Fig. 3). This turbulence flow reversal is localized to a radially narrow band of about 1 cm, outside of which the turbulence is again propagating in the ion diamagnetic direction. That configuration (LSN) has a lower *L-H* transition power threshold.

Profiles of the density fluctuation poloidal velocity and $E\times B$ velocity for the USN and LSN configurations are compared in Fig. 5. It is noted that the poloidal group velocities are not equal to the $E_r\times B_T$ velocities (inferred from charge exchange recombination spectroscopy measurements[5]), also shown in Fig. 5. First, there is no reversal in $E_r\times B_T$ velocity, and the magnitude is somewhat higher than the measured density fluctuation velocity. This implies that the turbulent density fluctuations are propagating in the plasma frame at a significant velocity in the electron diamagnetic direction. This may arise from intrinsic mode velocities (which are of the order of diamagnetic velocity) as would be expected of drift wave turbulence. The density fluctuation velocity shear and nonlinear decorrelation rates can be qualitatively compared. The density fluctuation velocity shear, estimated as $\omega_s\approx dV_\theta/dr$, is $\approx 8\times 10^5\ \mathrm{s}^{-1}$ in the high shear region. The measured nonlinear decorrelation rate of the turbulence, $1/\tau_c$, is in the range of $(0.3$–$2)\times 10^5\ \mathrm{s}^{-1}$. The decorrelation time τ_c is measured by the decay of the amplitude and increasing time lag of the peak cross correlation with increasing poloidal separation and reflects the average lifetime of the measured turbulent density fluctuations.[20] While a quantitative comparison of these quantities is difficult due to the dispersion and strongly nonlinear interactions of the fully saturated turbulence, the comparison shows that $\omega_s \gg 1/\tau_c$, and it is thus reasonable to expect that the density fluctuation poloidal velocity shear has a significant impact on the turbulence itself. The effective density fluctuation velocity shearing rate is much less elsewhere radially as well as in the USN plasma.

These observations demonstrate the dramatic differences in the edge turbulence characteristics between the two magnetic configurations discussed. The magnetic geometry and/or the ion ∇B drift direction clearly has a significant effect on the properties of the turbulence in this critical edge layer near the separatrix. Moreover, the dual-mode nature of the fluctuations (in LSN case only) is similar to observations on the Tokamak Fusion Test Reactor (TFTR),[21] where such double-mode propagation for the fluctuations was observed near the edge.[22] In contrast, however, the fluctuation propagation directions were different (perhaps due to different magnetic geometry; the TFTR plasma had a circular cross section and had a limiter). In the TFTR case, the higher frequency mode propagated in the electron diamagnetic direction, while the lower frequency mode propagated in the ion diamagnetic direction.

Interestingly, the amplitude of the density fluctuations are not dramatically different between the two configurations

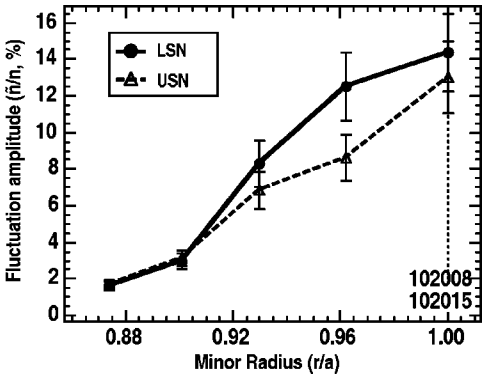

FIG. 6. Comparison of the density fluctuation amplitude profiles measured in both plasma configurations, USN (triangle symbols) and LSN (circle symbols).

in this L-mode condition. Figure 6 compares the profiles of rms amplitudes of fluctuation power. The LSN configuration exhibits a slightly higher amplitude near $r/a=0.96$, but over much of the profile, the amplitudes are rather similar and within the error bars. In the LSN case, the spectral power has been integrated over both the copropagating and counterpropagating modes.

III. SHEAR FLOW EFFECT ON DENSITY FLUCTUATION PROPERTIES

The wave number dispersion and radial correlation properties of the edge turbulence in the two magnetic configurations show distinct differences that are consistent with the variations in the density fluctuation velocity shear. This may partially explain the large difference in L-H transition power thresholds, though this is by no means conclusive. A biorthogonal decomposition analysis of coherent structures is used to show distinctions between turbulence structures in the two conditions.

The turbulence dispersion relations $k_\theta(\omega)$ are compared for both the LSN and USN configurations near the shear zone in Fig. 7. These dispersion relations have been inferred

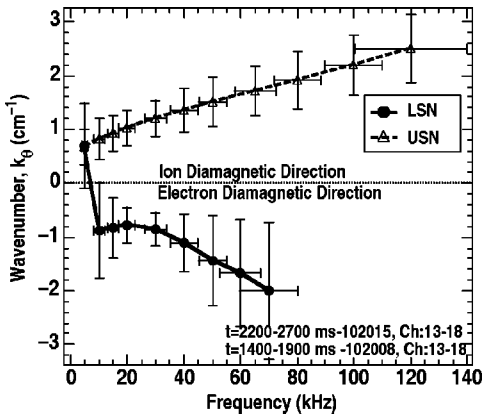

FIG. 7. Comparison of dispersion relations for turbulence in USN and LSN plasma at $r/a=0.93$, indicating substantial contrast. Positive (negative) poloidal wave numbers indicate propagation in the ion (electron) diamagnetic direction. Horizontal error bars represent frequency range filtered for that data point, while vertical bars represent the full-width at half-maximum of the associated $S(k_\theta)$ spectrum.

from a series of k_θ spectra, calculated using band-limited multipoint correlation analysis[23] at the radial location $\rho=0.93$. The horizontal error bars refer to the frequency band used for a given data point, while the vertical error bars refer to the half-width of the corresponding $S(k_\theta)$ spectrum. The USN and LSN configurations show dramatically different dispersion relations, illustrating the oppositely propagating modes in the two cases. Here $k_\theta>0$ refers to propagation in the ion diamagnetic direction while $k_\theta<0$ refers to propagation in the electron diamagnetic direction.

In the USN case, the turbulence shows that the wave number exhibits a roughly linearly increasing dependence on frequency. This result is consistent with the notion that different eddy scales are being more or less uniformly advected together, although there appears to be some moderate dispersion since a linear fit does not intercept the origin. The group velocity, taken as the slope of the curve, is nearly uniform for all modes. This is the velocity derived from the correlation analysis shown earlier in Fig. 5.

In the LSN condition, the dispersion relation is dramatically different and more complex, again illustrating the dual mode behavior. At the lowest frequencies and absolute wave numbers, the turbulence is propagating at nearly the same phase velocity as the USN condition, but then reverses direction at higher frequency, represented by negative wave numbers (which indicates propagation in the electron diamagnetic direction). This higher frequency mode in the LSN condition then exhibits a fairly uniform group velocity at increasing frequency.

The radial correlation functions of the turbulence are compared in Fig. 8, where the fluctuations located near and inside of $r/a\leqslant 0.93$, the location of the shear zone in the LSN case, are examined. The central channel of the poloidal array near $\rho=0.93$ is the reference channel, and for each function shown, six radial arrays at increasing poloidal locations in the 2D sampling array (Fig. 1) are averaged to improve statistics since all poloidally separated channels are at nearly the same radial location. The spatial spot size of the individual channels (about 0.8 cm width, radially) has been deconvolved from these correlation functions.

The radial correlation functions of the USN and LSN configurations are compared in Fig. 8(a). For the LSN configuration, the higher frequency mode is analyzed since the high and low frequencies have dramatically different radial correlations, discussed next. The high frequency band is also the one that experiences the dramatic flow reversal near the analyzed location. The radial correlation length, taken as the $1/e$ point of the radial correlation function, is sharply reduced in the LSN configuration (1.15 cm) relative to the USN configuration (1.80 cm). This result is qualitatively consistent with the increased poloidal velocity shear acting on turbulent eddies,[24] since the intrinsic poloidal velocity shear for this mode is much larger in the LSN case.

The two turbulent modes are compared for the LSN configuration in Fig. 8(b) and the radial correlation properties for the two modes are seen to be significantly different. The higher frequency mode (ion diamagnetic direction) exhibits a much smaller radial correlation length (1.15 cm), compared with the lower frequency mode (electron diamagnetic direc-

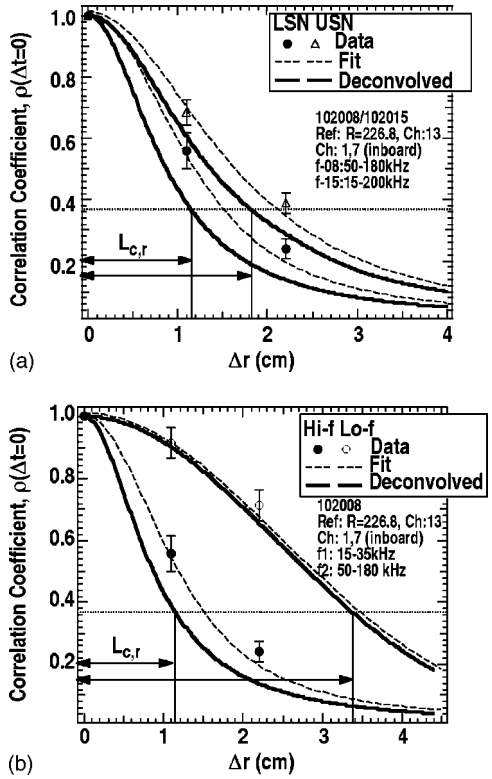

FIG. 8. (a) Radial correlation functions of USN turbulence and the higher frequency mode of the LSN turbulence (with spatial sampling resolution deconvolved), (b) comparison of the radial correlation functions for the high and low frequency modes in the LSN turbulence near $r/a=0.93$.

tion) which has a 3.3 cm correlation length. It is recalled that the higher frequency band experiences the sharp flow reversal or shear, while the lower frequency band does not show such a reversal and thus lower velocity shear. It is also noted that in general, lower frequency modes correspond to lower wave number and thus tend to exhibit longer correlation lengths. The dramatic difference in this case may be attributed to the different velocity shear experienced by the two modes.

The decorrelation times for the turbulence is measured to be of the order 10 μs for both configurations near the edge region. The turbulence decorrelation time ranges from 7 to 24 μs (from the inner channel towards the outer one) in the USN configuration. In the LSN configuration, it ranges from 5 to 35 μs (from the inner channel to the outer one).

To further compare the temporal and spatial characteristics of the edge turbulence dynamics, a biorthogonal decomposition (BD) algorithm has been applied to the 2D fluctuation data. The BD technique allows for the identification and isolation of coherent structures in the spatially and temporally resolved data, and is used here to compare and contrast the structure of the edge turbulence in the two magnetic configurations being examined. The technique realizes the projection of the data in an orthogonal basis in space and in time, allowing for the simultaneous analysis of the space and time dependencies of the fluctuation data. The method has been recently applied to the full 2D time- and space-resolved data, and details can be found in Refs. 18 and 25–27. The principle of the technique is quickly reviewed. Consider a

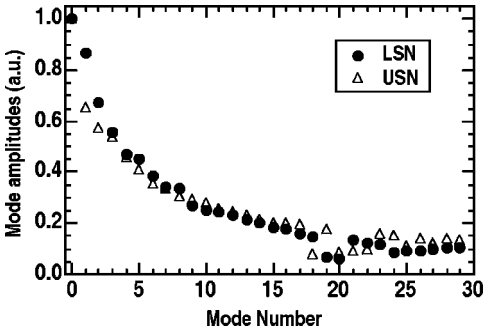

FIG. 9. Biorthogonal weighted component distributions for both configurations, upper-single-null (triangle symbols) and lower-single-null (circle symbols).

2D spatiotemporal signal $S(r,\theta,\mathrm{t})$ measured at N different spatial locations (r,θ) with M temporal frames. The data are assembled into an $N\times M$ array $S(z,\mathrm{t})$ where the columns contain the spatial information of the signal. Using a singular value decomposition algorithm, the biorthogonal decomposition technique expands the discrete data $S_{ij}=S(Z_j,t_i)$ into a unique set of modes that are orthogonal in time and in space so that $S_{ij}=\Sigma_{n=1}^{\min(N,M)}\lambda_n C_n(t_i)T_n(z_j)$ with $ST_n=\lambda_n C_n$. Here, λ_n, C_n, and T_n are, respectively, the weight component, the temporal component, and the spatial component [to be reshaped so that $T_n(z)=T_n(r,\theta)$] associated with the mode of order n[$=\min(N,M)$], eigensolutions, respectively, of the two-point temporal and the two-point spatial cross-correlation matrices of data matrix S. Thus, the higher the weight component, the stronger are the time and/or space correlations.

Figure 9 shows that the weight component distributions are similar for both magnetic configurations. As discussed in Refs. 18 and 25–27, the steepness of the distributions indicates a certain redundancy in the data, and implies that just a few modes are necessary to describe much of the data set. For either the USN or the LSN configuration, the first 14 modes represent over 90% of the signal power. The first ($n=1$) eigenmodes (which have the highest weight component) for both configurations are shown in Figs. 10 and 11 to compare the dominant spatial eigenfunctions. The related spatial components are rather different [Figs. 10(a) and 11(a)]. Moreover, in the USN configuration, the temporal component exhibits a large-scale structure distribution associated with low frequency components [Fig. 10(b)]. In the LSN configuration, that large-scale structure is no longer apparent [Fig. 11(b)]. This result is qualitatively consistent with the results from radial correlation analyses that the inherent flow shear acts to reduce turbulent structure sizes.

Finally, note that as the mode number n increases, the mode spatial structure tends to oscillate with increasing wave number, and the associated temporal component exhibits a higher frequency distribution, the latter being ultimately increasingly dominated by noise.

IV. DISCUSSION

The stabilization of L-mode turbulence by $E_r\times B_T$ shear flow has been the dominant paradigm to explain the L-mode

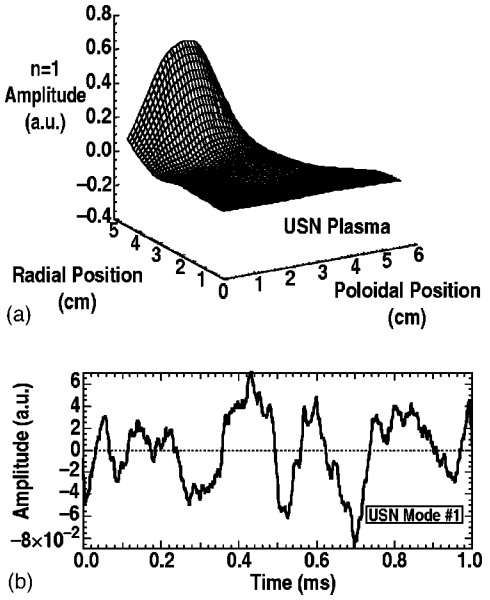

FIG. 10. Lowest order mode of biorthogonal decomposition of edge density fluctuations for upper-single-null plasma, (a) spatial component, (b) temporal component.

to *H*-mode transition.[4,5,28–31] Sheared flows are expected to act on turbulent eddies by reducing their radial correlation length, hence the radial step length for turbulent transport as well as by decorrelating the density and potential fluctuations. For the experiments reported here, our observations are consistent with the picture of turbulence stabilization by shear in the poloidal group velocity of density fluctuations. In the case with lower density fluctuation velocity shear (USN configuration), a larger-scale distribution for turbulent structures is observed. With higher fluctuation poloidal velocity shear (LSN configuration), a smaller-scale structure distribution is apparent, with reduced radial correlation lengths as well as decorrelation times. However, the corresponding $E_r \times B_T$ velocities are found to be somewhat higher in magnitude than the fluctuation poloidal group velocities. Notably, there is no $E_r \times B_T$ flow reversal. This observation suggests that in these cases, shear in the total density fluctuation flow velocity (not just that in the $E_r \times B_T$ velocity), may be crucial to the *L-H* transition dynamics.

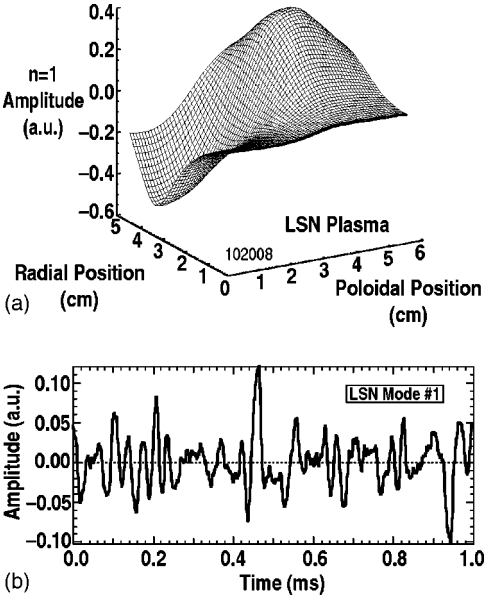

FIG. 11. Lowest order mode of biorthogonal decomposition of edge density fluctuations for lower-single-null plasma, (a) spatial component, (b) temporal component.

Theoretical models generally predict that it is the $E_r \times B_T$ velocity (rather than the fluid velocity) that is held to be responsible for turbulence suppression.[32–34] We note that recent nonlinear simulations with the continuum gyrokinetic code GYRO (Ref. 35) suggest that it is not only the $E \times B$ velocity shear that is important for turbulence stabilization, but that shear in the intrinsic mode phase velocities may also contribute to turbulence stabilization.[36] In this case, the total shear, including that in the $E \times B$ and intrinsic phase velocity, is used to help explain the breaking of gyro-Bohm transport due to profile shear stabilization. Hence, our observations suggest that shear in the density fluctuation velocity may play a role in turbulence suppression at the *L-H* transition. Although the onset of the observed naturally occurring poloidal flow reversal in the LSN configuration is not yet understood, it appears that it may affect the *L-H* transition power threshold because of the more favorable density fluctuation flow shear in this critical edge region.

We note that a model of the *L-H* transition based on zonal flow generation by finite beta drift waves in the edge of tokamak plasmas has shown remarkably good agreement with a database of *L-H* transitions observed in DIII-D discharges.[11] This model predicts that as an edge parameter, $\Theta = T_e/\sqrt{L_n}$, exceeds a critical value, Θ_c (dependent on plasma parameters and tokamak geometry), *L-H* transition should occur. These experimental observations of the naturally occurring turbulence flow shear may be a manifestation of the zonal flow and zonal field generation that is predicted to trigger the *L-H* transition. The slight differences in the edge electron density, temperature, and pressure [Figs. 2(a)–2(c)] may be consistent with such a transition mechanism (recent experimental measurements with a density profile reflectometer system on DIII-D are allowing for a detailed comparison of density gradients in upper- and lower-signal-null discharges.[37] On the other hand, these measurements presented here are of a mean density fluctuation velocity shear, in contrast to the time-varying dynamics of zonal flows.

Also, we note that recent experimental measurements of scrape-off-layer flows in the C-MOD tokamak show sharp differences between plasmas with similar magnetic equilibria to those studied here, and likewise suggest a flow-related mechanism to explain the large differences in *L-H* transition power.[38] Indeed it might be that scrape-off-layer flows are in some way related to or interact with the near-edge density fluctuation flows as observed here. This should be the subject of future investigations.

Other theoretical studies have shown the importance of the interaction between mean shear flows, zonal flows, ambient turbulence, and the edge pressure gradient in determining the *L-H* transition dynamics.[39] Here, zonal flows are also shown to be the *L-H* transition trigger mechanism, and mean

shear flow is actually shown to slightly increase the required power for the *L-H* transition by inhibiting the growth of zonal flows. Future experiments will aim to quantitatively compare theoretical models and experimental measurements of mean and time-varying turbulence flow shear (e.g., zonal flows, including geodesic acoustic modes[40]), ambient turbulence, and the local pressure gradient.

These observations presented here also show some consistency with recent simulations of edge turbulence.[41] First, the simulations predict the fluctuation flow reversal at the edge in the LSN configuration. Second, the calculated fluctuation phase velocities contrast with $E_r \times B_T$ velocities. Finally, oblique structures are observed in the LSN configuration—the lower LH transition power threshold condition—as in *H*-mode case simulations.

V. SUMMARY

A dramatic change in the poloidal flow direction of density fluctuations near the plasma edge, and correspondingly large natural flow shear, has been observed in *L*-mode DIII-D plasmas when the ∇B drift is directed towards the *X* point (lower-single-null configuration). This configuration corresponds to the magnetic configuration with the lower *L-H* transition power threshold. In contrast with the upper-single-null configuration (∇B drift away from the *X* point), the fluctuations exhibit counterpropagating modes (with a dominant flow drifting in the ion diamagnetic direction) inside the flow reversal layer, and a single-mode behavior outside. The fluctuation characteristics inferred from cross-correlation analyses indicate that the turbulence properties differ substantially for the two configurations. Combined with the analysis of the fluctuation data in terms of biorthogonal decomposition modes, our results show that the large-scale turbulent structure distribution observed in the upper-single-null configuration is no longer apparent in the lower-single-null configuration. Reduced radial correlation lengths and decorrelation times are observed, suggesting a flow shear that may act to stabilize turbulence. Moreover, the $E_r \times B_T$ velocities are found to be somewhat higher than the fluctuation poloidal group velocities and do not exhibit such a flow reversal in the *L*-mode phase. This suggests that the density fluctuation velocity shear may be a key parameter affecting the *L-H* transition power. Hence, the transition would occur at lower input power (LSN configuration) because of more favorable plasma turbulence conditions near the edge given the natural flow shear observed in the fluctuation poloidal velocity.

An understanding of the fluctuation flow shear generation mechanism at the plasma edge, and its dependence on the magnetic configuration will be the subject of future investigations.

ACKNOWLEDGMENTS

The authors thank R. E. Waltz, X. Garbet, W. Nevins, and X. Xu for useful discussions regarding the interpretation of these measurements.

This work was supported by the U.S. Department of Energy under Grant No. DE-FG02-89ER53296 and Contract No. DE-AC03-99ER54463, and by Direction Générale de la Coopération Internationale et du Développement (DGCID) of France under the scientific program Lavoisier.

[1] F. Wagner, G. Becker, K. Behringer *et al.*, Phys. Rev. Lett. **49**, 1408 (1982).
[2] K. H. Burrell, E. J. Doyle, P. Gohil *et al.*, Phys. Plasmas **1**, 1536 (1994).
[3] J. A. Boedo, D. S. Gray, P. W. Terry, S. Jachmich, G. R. Tynan, R. W. Conn, and TEXTOR-94 Team, Nucl. Fusion **42**, 117 (2002); G. R. Tynan, L. Schmitz, L. Blush *et al.*, Phys. Plasmas **1**, 3301 (1994).
[4] R. A. Moyer, K. H. Burrell, T. N. Carlstrom *et al.*, Phys. Plasmas **2**, 2397 (1995).
[5] K. H. Burrell, Phys. Plasmas **4**, 1499 (1997).
[6] T. Fukada, Plasma Phys. Controlled Fusion **40**, 543 (1998).
[7] R. J. Groebner and T. N. Carlstrom, Plasma Phys. Controlled Fusion **40**, 673 (1998).
[8] T. N. Carlstrom and R. J. Groebner, Phys. Plasmas **3**, 1867 (1996).
[9] R. J. Groebner, D. M. Thomas, and R. D. Deranian, Phys. Plasmas **8**, 2722 (2001).
[10] R. D. Deranian, R. J. Groebner, and D. T. Pham, Phys. Plasmas **7**, 1235 (2000).
[11] P. N. Guzdar, R. G. Kleva, R. J. Groebner, and P. Gohil, Phys. Rev. Lett. **89**, 265004 (2002); Phys. Plasmas **11**, 1109 (2004).
[12] J. W. Connor and H. R. Wilson, Plasma Phys. Controlled Fusion **42**, R1 (2000).
[13] T. N. Carlstrom, P. Gohil, J. G. Watkins, K. H. Burrell, S. Coda, E. J. Doyle, R. J. Groebner, J. Kim, R. A. Moyer, and C. L. Rettig, Plasma Phys. Controlled Fusion **36**, A147 (1994).
[14] L. D. Horton, Plasma Phys. Controlled Fusion **42**, A37 (2000).
[15] T. N. Carlstrom, R. J. Groebner, C. Fenzi, G. R. McKee, R. A. Moyer, and T. L. Rhodes, Plasma Phys. Controlled Fusion **44**, A333 (2002).
[16] G. R. McKee, R. Ashley, R. Durst, R. Fonck *et al.*, Rev. Sci. Instrum. **70**, 913 (1999).
[17] R. J. Fonck, P. A. Duperrex, and S. F. Paul, Rev. Sci. Instrum. **61**, 3487 (1990).
[18] C. Fenzi, R. J. Fonck, M. Jakubowski, and G. R. McKee, Rev. Sci. Instrum. **72**, 988 (2001).
[19] G. R. McKee, C. Fenzi, R. J. Fonck, and M. Jakubowski, Rev. Sci. Instrum. **74**, 2014 (2003).
[20] R. D. Durst, R. J. Fonck, G. Cosby, H. Evensen, and S. F. Paul, Rev. Sci. Instrum. **63**, 4907 (1992).
[21] D. Meade and The TFTR Group, *Proceedings of the International Conference on Plasma Physics and Controlled Nuclear Fusion, Washington, DC, 1990* (International Atomic Energy Agency, Vienna, 1991), Vol. I, pp. 9–14.
[22] R. D. Durst, R. J. Fonck, J. S. Kim, S. F. Paul, N. Bretz, C. Bush, Z. Chang, and R. Hulse, Phys. Rev. Lett. **71**, 3135 (1993).
[23] R. J. Fonck, G. Cosby, R. D. Durst, S. F. Paul, N. Bretz, S. Scott, E. Synakowski, and G. Taylor, Phys. Rev. Lett. **70**, 3736 (1993).
[24] P. W. Terry, Rev. Mod. Phys. **72**, 109 (2000).
[25] T. Dudok de Wit, A.-L. Pecquet, J.-C. Vallet, and R. Lima, Phys. Plasmas **1**, 3288 (1994).
[26] S. Benkadda, T. Dudok de Wit, A. Verga, A. Sen, ASDEX Team, and X. Garbet, Phys. Rev. Lett. **73**, 3403 (1994).
[27] T. Dudok de Wit, Plasma Phys. Controlled Fusion **37**, 117 (1995).
[28] P. H. Diamond, Y.-M. Liang, B. A. Carreras, and P. W. Terry, Phys. Rev. Lett. **72**, 2565 (1994).
[29] B. A. Carreras, L. W. Owen, R. Maingi, P. K. Mioduszewski, T. N. Carlstrom, and R. J. Groebner, Phys. Plasmas **5**, 2623 (1998).
[30] A. L. Rogister, Trans. Fusion Technol. **37**, 287 (2000).
[31] J. Hugill, Plasma Phys. Controlled Fusion **42**, R75 (2000).
[32] H. Biglari, P. H. Diamond, and P. W. Terry, Phys. Fluids B **2**, 1 (1990).
[33] A. B. Hassam, T. M. Antonsen, Jr., J. F. Drake, P. N. Guzdar, C. S. Liu, D. R. McCarthy, and F. L. Waelbroeck, Phys. Fluids B **5**, 2519 (1993).
[34] J. N. Le Boeuf, L. A. Charlton, and B. A. Carreras, Phys. Fluids B **5**, 2959 (1993).
[35] J. Candy and R. E. Waltz, J. Comput. Phys. **186**, 545 (2003).
[36] R. E. Waltz, J. M. Candy, and M. N. Rosenbluth, Phys. Plasmas **9**, 1938 (2002).
[37] G. Wang, T. L. Rhodes, E. J. Doyle, W. A. Peebles, L. Zeng, K. H. Burrell, G. R. McKee, R. J. Groebner, and T. E. Evans, Plasma Phys. Controlled Fusion **46**, A363 (2004).
[38] B. LaBombard, Bull. Am. Phys. Soc. **49** (8), 97 (2004).

[39] E. J. Kim and P. H. Diamond, Phys. Rev. Lett. **90**, 185006 (2003).
[40] M. Jakubowski, R. J. Fonck, and G. R. McKee, Phys. Rev. Lett. **89**, 265003 (2002); G. R. McKee, R. J. Fonck, M. Jakubowski *et al.*, Phys. Plasmas **10**, 1712 (2003); G. R. McKee, R. J. Fonck, M. Jakubowski, K. H. Burrell, K. Hallatschek, R. A. Moyer, W. Nevins, D. L. Rudakov, and X. Xu, Plasma Phys. Controlled Fusion **45**, A477 (2003).
[41] X. Q. Xu, R. H. Cohen, T. D. Rognlien, and J. R. Myra, Phys. Plasmas **7**, 1951 (2000).